International Journal of Emerging Engineering Research and Technology
Volume 8, Issue 2, 2020, PP 17-22
ISSN 2349-4395 (Print) & ISSN 2349-4409 (Online)

The Point Spread Function of an Aperture in the Form of Corona Virus (COVID 19) Images

A. M. Hamed*

Physics Department, Faculty of Science, Ain Shams University, 11566 Cairo, Egypt

***Corresponding Author:** A. M. Hamed, Physics Department, Faculty of Science, Ain Shams University, 11566 Cairo, Egypt.*

ABSTRACT

In this paper, an aperture in the form of Coronavirus is suggested. Two models are given to represent the aperture where the circular part has linear distribution in both models and surrounded by eight equal circles of very small diameter. The small circles, in the 1st model, has linear distribution while in the 2nd model Hamming distribution is assumed. The Point Spread Function PSF is computed in both models and compared with the PSF in case of uniform aperture. The Fourier spectrum of the COVID 19 is computed and plotted. In addition, the autocorrelation is computed in all cases and compared with the autocorrelation function corresponding to the Coronavirus image. The Mat- Lab codes are used in the computation of all images and plots.

Keywords: *Coronavirus (COVID 19), modulated aperture, Point Spread Function (PSF), autocorrelation.*

INTRODUCTION

The concept of modulation applied on microscopic apertures is previously investigated by many authors [1- 10] since they studied the amplitude filters obstructed by either rectangular or circular and annular apertures seeking to attenuate the intensity in the outer rings of the diffraction pattern. Many authors investigated the aperture modulation in confocal microscopes by Sheppard et.al.[11- 15] and by Clair and A. Hamed [16-19], using linear and quadratic apertures. Recently, different models of aperture modulation are presented by A. Hamed [20- 25] using Hamming and elliptic and other modified apertures and showing its effect on microscope resolution. Image analysis of modified Hamming aperture and its application on confocal microscopy and holography is given [23].

Recently, design of a Cascaded Black – Linear Distribution (CBLD) in circular aperture and its Application on Confocal Laser Scanning Microscope (CSLM) is presented [24].

In this study, the pandemic COVID 19 virus has particles approximated by a circular disc assumed of linear distribution surrounded by very small circles of linear or Hamming or any other distribution. Hence, two models are presented in this study and the PSF is computed and investigated as well as the autocorrelation of the assumed models of coronavirus. Theoretical presentation for the models is given followed by results and discussion and finally a conclusion is presented.

THEORETICAL ANALYSIS

The 1st model of Coronavirus composed of eight equal circles of linear distribution placed on the surface of a circle of linear distribution with radius = ρ_L while the small circles surrounding the central circle each of radius = $\alpha\rho_L$where $\alpha << 1$ as shown in the figure (1).

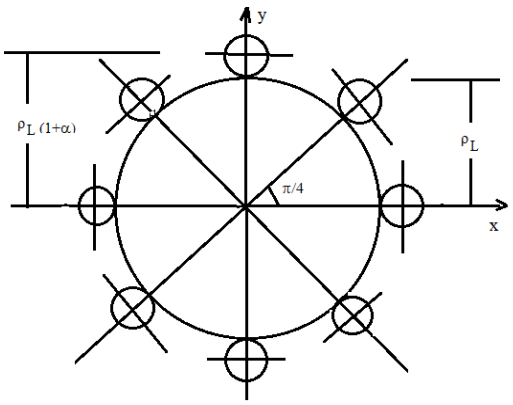

Figure1. *An aperture in the form of central circular core of linear distribution surrounded from outside by eight equal circles each of radius = $\alpha\rho_L$, where $\rho_L$is the core radius and α <<1. The eight circles are chosen to be either linear distribution or having Hamming distribution.*

The model of the aperture shown in the figure (1) is assumed similar to COVID 19cell. It is mathematically represented as follows:

$$P_{covid\ 19}(x,y) = P_L(x,y) + \sum_{i=1}^{2} P_i\,[x,\ y \pm \rho_L(1+\alpha)] + \sum_{j=3}^{4} P_j\,[x \pm \rho_L(1+\alpha), y] + \sum_{k=5}^{8} P_k\,[x \pm \rho_L(1+\alpha),\ y \pm \rho_L(1+\alpha)] \quad (1)$$

The central disc with linear distribution has radius = ρ_L and is described as follows:

$$P_L(\rho) = \rho \quad \text{for} \left|\frac{\rho}{\rho_L}\right| \le 1 \quad (2)$$

where the radial coordinate $\rho = \sqrt{x^2 + y^2}$ and x, y are the Cartesian coordinates in the aperture plane. The other eight equal circles have the same linear distribution but shifted according to equation (1).

Equation (1), can be rewritten using the properties of Dirac- delta function and convolution operation as follows:

$$P_{covid\ 19}(x,y) = \rho + P_1(\rho/\alpha) \otimes \{[\sum_{i=1}^{2} \delta[x,\ y \pm \rho_L(1+\alpha)] + \sum_{i=3}^{4} \delta[x \pm \rho_L(1+\alpha), y] + \sum_{i=5}^{8} \delta\,[(x \pm \rho_L(1+\alpha))/\sqrt{2},\ (y \pm \rho_L(1+\alpha))/\sqrt{2}]\,]\} \quad (3)$$

Where $\otimes$ is a symbol for convolution operation and $\alpha = \frac{1}{8}$.

The Point Spread function of the COVID 19 aperture represented by equation (3) is computed by operating the FT and making use of the convolution properties which is transformed into simple product of one of the small apertures of linear distribution and radius = $\alpha\rho_L$ and the inclined exponential phase shifts. Hence, we get this result:

$$h_{covid\ 19}(u,v) = \text{F.T.}\{\rho\} + \text{F.T.}\left\{P_1\left(\frac{\rho}{\alpha}\right)\right\}.F.T.\{\sum_{i=1}^{2} \delta[x,\ y \pm \rho_L(1+\alpha)] + \sum_{i=3}^{4} \delta[x \pm \rho_L(1+\alpha), y] + \sum_{i=5}^{8} \delta\,[(x \pm \rho_L(1+\alpha))/\sqrt{2},\ (y \pm \rho_L(1+\alpha))/\sqrt{2}]\} \quad (4)$$

Since

$$F.T.\{\rho\} = 4\pi\,\{\frac{J_1(W)}{W} + \frac{J_0(W)}{W^2} - 2\sum_i \frac{J_i(W)}{W^3}\} \quad (5)$$

with i = 1, 3, 5, … and W is the reduced coordinate given as follows: $W = \frac{2\pi r\,\rho_L}{\lambda f}$ where ρ_L is the radius of the central disc as stated before.

Similarly, the F.T. of the small apertures of radius = $\alpha\rho_L$ is computed to give this result:

$$F.T.\{\rho\} = 4\pi\,\{\frac{J_1(\alpha W)}{\alpha W} + \frac{J_0(\alpha W)}{(\alpha W)^2} - 2\sum_i \frac{J_i(\alpha W)}{(\alpha W)^3}\} \quad (6)$$

Since F.T. $\{\delta[x,\ y \pm \rho_L(1+\alpha)]\}\exp\{\left(\frac{j2\pi}{\lambda f}\right)(1+\alpha)\rho_L v\}$ and similar expressions are obtained giving cosine function for each two symmetric apertures. Substitute equations (5), and (6) in equation (4), we finally get this result for the PSF written as follows:

$$h_{covid\ 19}(u,v) = \{\frac{J_1(W)}{W} + \frac{J_0(W)}{W^2} - 2\sum_i \frac{J_i(W)}{W^3}\} + 2\{\frac{J_1(\alpha W)}{\alpha W} + \frac{J_0(\alpha W)}{(\alpha W)^2} - 2\sum_i \frac{J_i(\alpha W)}{(\alpha W)^3}\}.\left\{\left[\cos\left(\frac{2\pi}{\lambda f}\right)(1+\alpha)\rho_L v\right] + \left[\cos\left(\frac{2\pi}{\lambda f}\right)(1+\alpha)\rho_L u\right] + \left[\cos\frac{\left(\frac{2\pi}{\lambda f}\right)(1+\alpha)\rho_L(u+v)}{\sqrt{2}}\right] + \left[\cos\frac{\left(\frac{2\pi}{\lambda f}\right)(1+\alpha)\rho_L(u-v)}{\sqrt{2}}\right]\right\} \quad (7)$$

The 2nd model has the same shape as shown in the figure (1) while the eight circles have Hamming distribution. Following the same analysis except we compute the F.T. of one of the small circles which have Hamming distribution. In case of the Hamming apertures surrounding the central disc of linear distribution, the aperture is represented as follows:

$$P_{covid\ 19}(x,y)_{ham} = \rho + \left\{0.54 + 0.46\cos\left[\beta\pi\sqrt{x^2 + (y \pm \rho_L(1+\alpha))^2}\right]\right\} + \left\{0.54 + 0.46\cos\left[\beta\pi\sqrt{(x \pm \rho_L(1+\alpha))^2 + y^2}\right]\right\} + \left\{0.54 + 0.46\cos\left[\left(\frac{\beta\pi}{\sqrt{2}}\right)\sqrt{(x \pm \rho_L(1+\alpha))^2 + (y \pm \rho_L(1+\alpha))^2}\right]\right\} \quad (8)$$

Where the 1st part in the L.H.S. ρ represents the central disc of linear distribution, while the 2nd part represents the two hamming circles located along the y- axis at $y = \pm\rho_L(1+\alpha)$, and the 3rdpart represents the two hamming circles located along the x- axis at $x = \pm\rho_L(1+\alpha)$, and the 4th term contains four hamming circles located at $x = \pm\rho_L(1+\alpha)/\sqrt{2}$, $y = \pm\rho_L$

Operating the FT. upon equation (8) and making use of the convolution products of Shifted Dirac-Delta function we get the PSF as follows:

$$h_{covid\ 19}(u,v)_{ham} = \{\frac{J_1(W)}{W} + \frac{J_0(W)}{W^2} - 2\sum_i \frac{J_i(W)}{W^3}\} + \left\{0.54\,\delta(r) + 0.23\left[\delta_1\left(r - \frac{\beta\lambda f}{2}\right) + \delta_2\left(r + \frac{\beta\lambda f}{2}\right)\right]\right\}.\left\{\left[\cos\left(\frac{2\pi}{\lambda f}\right)(1+\alpha)\rho_L v\right] + \left[\cos\left(\frac{2\pi}{\lambda f}\right)(1+\alpha)\rho_L u\right] + \left[\cos\frac{\left(\frac{2\pi}{\lambda f}\right)(1+\alpha)\rho_L(u+v)}{\sqrt{2}}\right] + \left[\cos\frac{\left(\frac{2\pi}{\lambda f}\right)(1+\alpha)\rho_L(u-v)}{\sqrt{2}}\right]\right\} \quad (9)$$

RESULTS AND DISCUSSION

In this section, we compute the Fourier spectrum corresponding to the COVID 19 virus particles seeking to model it in the described form shown in the figure (1). The central disc is assumed has linear distribution while the surrounding small circles have either linear or Hamming distributions and comparison with the uniform distribution of the aperture is given.

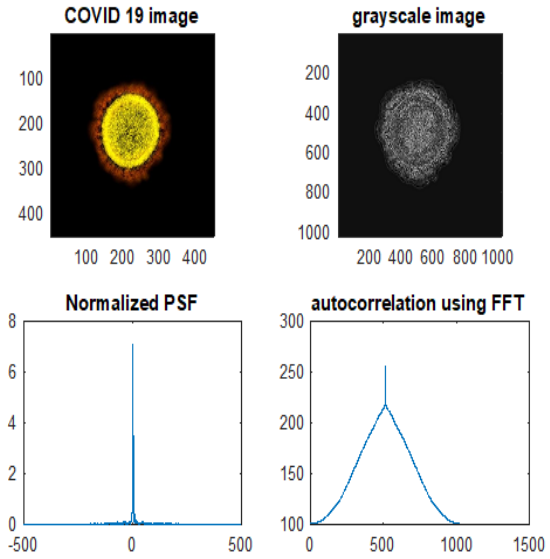

Figure2a. *In the 1st row a color and its corresponding grayscale images are shown for the COVID 19 virus particle, while in the 2nd row in the left the normalized PSF and in the right the autocorrelation of the input image is plotted.*

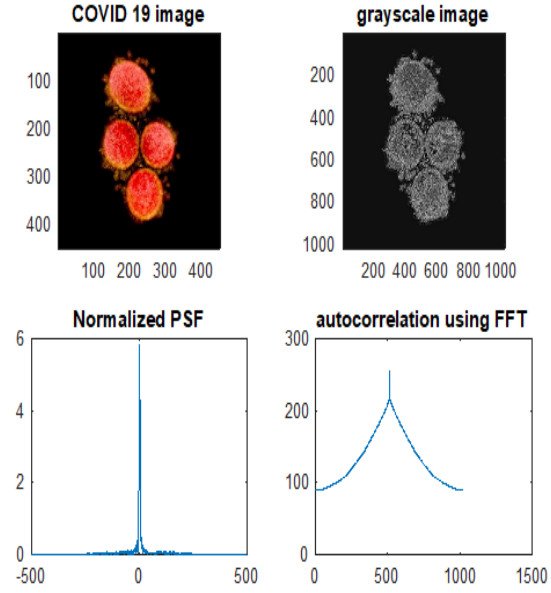

Figure2b. *The PSF and the autocorrelation of the Coronavirus image having four particles are shown.*

In the 1st row a color image and its corresponding grayscale image are shown for the COVID 19 virus particle, while in the 2nd row in the left the normalized PSF and in the right the autocorrelation of the input image is plotted as shown in the figure (2- a). Similar results are plotted for the four particles of coronavirus as shown in the figure (2- b). It is noted that the grayscale images are rescaled to dimensions 1024 ×1024 pixels. It is shown that central peak is affected by some peaks located in contact with the central peak nearly three peaks are appeared. In addition, the autocorrelation peak corresponding to the coronavirus particle shown in the figure (2- a) is computed from the plot giving this value:

BW $_{plot}$ = 1000 pixels compared with the cell dimension = 477 pixels giving value BW=477× 2 = 954 pixelswith error = 4.6%.

Now we examine the Fourier spectrum obtained from the described models or the normalized PSF.

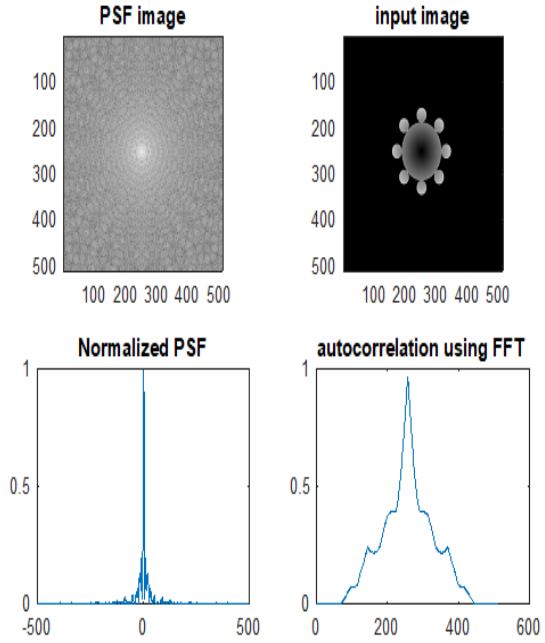

Figure3.

The input image in the1st model of Coronavirus where the central disc of linear distribution has radius = 64 pixels while the surrounding eight circles have radii = 16 pixels is used in the computation of the PSF and autocorrelation plots as shown in the figure (3). It is noted that, the normalized PSF corresponding to the aperture and the autocorrelation of the input image are computed using the FFT technique. In the autocorrelation plot corresponding the model 1, linear part is shown in the center surrounded by irregular shape due to the presence of the surrounding separated small circles of linear distribution. The band width computed from the plot is calculated as follows:

BW $_{auto\ correl.}$ = (central radius + small circle radius) ×4 = (64 + 16) × 4 = 320 pixels

Similar plots of the PSF and autocorrelation for the model 1 at central disc = 64 pixels while the small circles of radii = 8 pixels are given in the figure (4). While the PSF and autocorrelation at central disc = 32 pixels and the surrounding small circles have radii = 4 pixels for the same model 1 are plotted as in the figure (5).

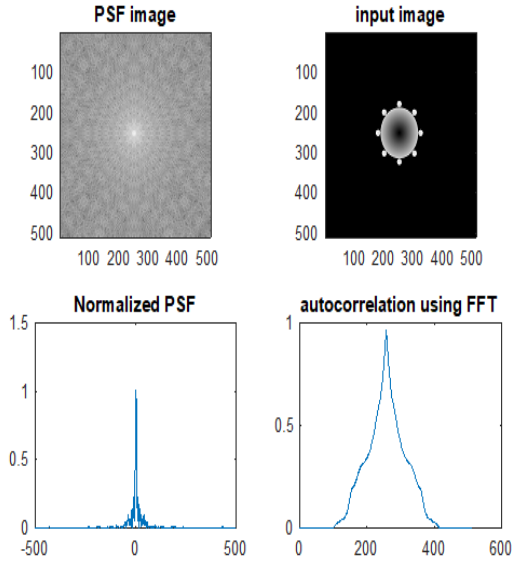

Figure4.

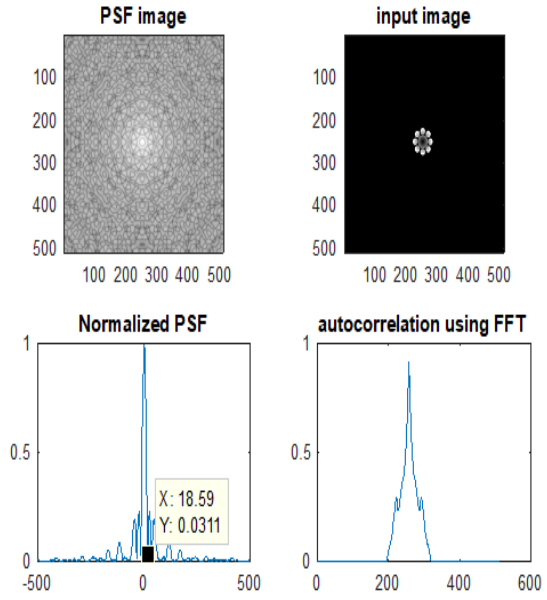

Figure5.

The band width computed from the input image in the figure (4) as follows:

BW = = (64 + 8) × 4 = 288 pixels

While the BW computed from the image shown in the figure (5) is:

BW = = (32 + 4) × 4 = 144 pixels

It is shown that the autocorrelation BW is two times the external diameter of the aperture including the small circles.

It is shown, referring to the normalized PSF plot in the figure (5), that the cut-off spatial frequency $r_c/\lambda f$ = 18.59 nm/λf and four legs of moderate values around the central peak are shown which is useful for imaging extended objects.

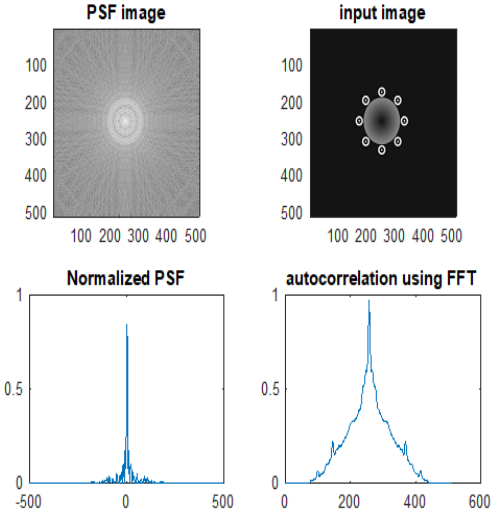

Figure6.

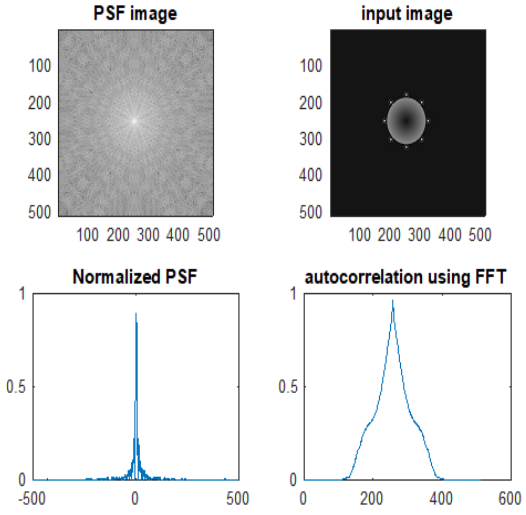

Figure7.

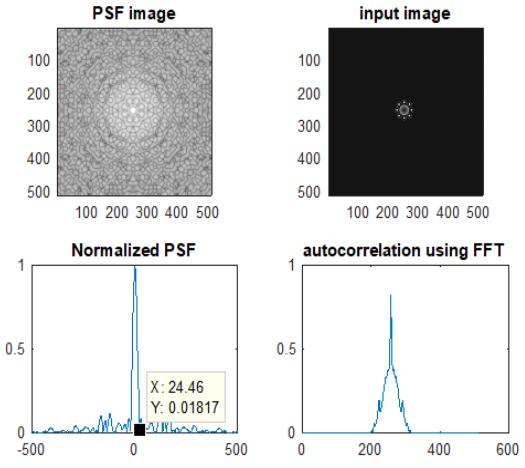

Figure8.

Similar plots are shown in the figures (6, 7, 8) for the 2nd model where the eight small circles surrounding the central peak have Hamming distribution while the central disc kept of linear distribution. The cut- off spatial frequency computed from the normalized PSF shown in the figure (8) is $r_c/\lambda f$ = 24.46 nm/λf while the secondary peaks around the central peak are distributed equally in a larger range as expected from the Hamming distributions of the small circles placed around the central disc. It is noted that all the plots of the PSF shown in the figures (3 →9) are taken at the center of the pattern at y = 256 pixels.

A comparative model (without modulation inside the circles) of Coronavirus is assumed. It is composed of eight equal circles of uniform distribution placed on the surface of a circle of uniform distribution and radius = 32 pixels while the small circles each of radius = 4 pixels as shown in the figure (9). The normalized PSF for the aperture shown in the figure (9) versus the radial coordinate is computed and plotted. The cut-off spatial frequency $r_c/\lambda f$ = 20.55 nm/λf is shown where it has moderate cut- off shown between the cut- off spatial frequency of the PSF in the linear distribution (figure 5) and the PSF in the Hamming distribution (figure 8). Hence, we write this result:

$(r_c/\lambda f)_{Ham.}$ =24.46 nm > $(r_c/\lambda f)_{circle}$ =20.55 nm > $(r_c/\lambda f)_{linear}$ =24.46 nm.

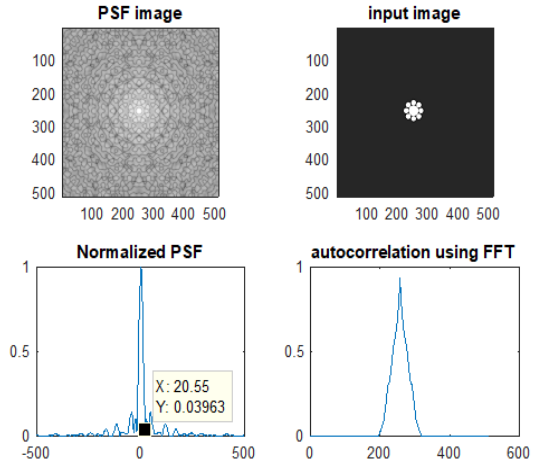

Figure9.

In addition, referring to all images obtained in case of small linear disc of radius = 32 pixels where each small circle has radius = 4 pixels, as in figure (5) for linear distribution, figure (8) for Hamming distribution, and figure (9) for uniform circular disc surrounded by uniform circles, it is shown that the PSF images have uniform regular shapes.

It is noted that the BW corresponding to the model 2 have the same values like in the model 1 since the same dimensions are assumed in both models. No irregularity in the autocorrelation plot in case of no modulation as compared with the plots shown in the models 1, 2 depending on the value of the radii of the small circles.

CONCLUSION

Firstly, a design of two models of apertures similar to COVID 19 virus particle are executed. The PSF corresponding to these novel apertures is computed and compared with similar arrangement in absence of modulation. The 1st model composed of central disc of linear distribution surrounded by eight small circles of the same distribution has cut- off spatial frequency narrower than that corresponding to the 2nd model where the small circles are assumed of Hamming distribution. While in case of no modulation, the cut-off spatial frequency lies between the two values corresponding to the two models.

Secondly, all the PSF images showed a central spot surrounded by diffracting pattern which has resemblance with the number of circles surrounding the central disc.

The autocorrelation plots corresponding to the models 1, 2 have irregularity around the central uniform peak due to the distribution either linear or Hamming of the small circles. Uniform conic shape is obtained in case of the model with uniform circles, hence no modulation is present.

REFERENCES

[1] G. Lansraux, Rev. Opt. Theor. Instr. 34, 65 (1955).

[2] H.H. Hopkins, Proc. Phys. Soc. London B, 62,22 (1949).

[3] H.H. Hopkins, Opt. Acta 2, 23 (1955).

[4] A. Boivin, Theorie et calcul des figures de diffraction de revolution, Laval, U.P. Quebec (1964).

[5] T. Wilson and D.K. Hamilton, J. microscopy 128, 139 (1982).

[6] C.J.R. Sheppard, D.K. Hamilton, and I.J. Cox, Proc. R Soc. (London) A387,171 (1983).

[7] T. Wilson and C.J.R. Sheppard, Theory and practice of Scanning Optical Microscope, Academic Press INC (London) 1984.

[8] D.K. Hamilton, T. Wilson, and C.J.R. Sheppard, Opt. Lett.6, 625 (1981).

[9] G.W. Goodman, Introduction to Fourier optics, McGraw Hill Book comp., New York (1968).

[10] G. Nomarski, J. Opt. Soc. Am., 65, 1166 (1975).

[11] C.J.R. Sheppard, and A. Choudhary, Opt. Acta 24, 1051(1977).

[12] T. Wilson, and C.J.R. Sheppard, Opt. Acta 26, 761(1979).

[13] C.J.R. Sheppard and T. Wilson, Opt. Acta 27, 611 (1980).

[14] I.J. Cox, C.J.R. Sheppard, and T. Wilson, Appl. Opt. 21, 778 (1982).

[15] D.K. Hamilton, and T. Wilson, J. Appl. Phys. 53, 5321(1982).

[16] J. J. Clair and A. M. Hamed, Optik 64, 133(1983).

[17] A. M. Hamed and J. J. Clair, Optik 64, 277(1983).

[18] A. M. Hamed and J. J. Clair, Optik 65, 209 (1983).

[19] A.M. Hamed, Opt.& Laser Tech. 16, 93 (1984).

[20] A.M. Hamed, Journal of Modern optics, 56, 1174 (2009).

[21] A.M. Hamed, Journal of Modern optics, 56, 1633 (2009).

[22] A.M. Hamed, Optik, 131, 838 (2017).

[23] A.M. Hamed and T.A. Al-Saeed, J. Modern Opt. 62, 801(2015).

[24] AM. Hamed, Am. J. Optics & Photonics 3 (2019)

[25] A. M. Hamed, www.lap.com (Lambert Academic Publishing), 14 Nov. (2017), The Point Spread Function of some modulated apertures (Application on speckle and interferometry images) ISBN: 9786202070706.

Citation: *A. M. Hamed, "The Point Spread Function of an Aperture in the Form of Coronavirus (COVID 19) Images", International Journal of Emerging Engineering Research and Technology, 8(2), 2020, pp. 17-22.*